

# Plan, Verify and Fill: A Structured Parallel Decoding Approach for Diffusion Language Models

Miao Li <sup>\*1</sup> Hanyang Jiang <sup>\*1</sup> Sikai Cheng <sup>1</sup> Hengyu Fu <sup>2</sup> Yuhang Cai <sup>2</sup> Baihe Huang <sup>2</sup> Tinghan Ye <sup>1</sup>  
 Xuanzhou Chen <sup>1</sup> Pascal Van Hentenryck <sup>1</sup>

## Abstract

Diffusion Language Models (DLMs) present a promising non-sequential paradigm for text generation, distinct from standard autoregressive (AR) approaches. However, current decoding strategies often adopt a reactive stance, underutilizing the global bidirectional context to dictate global trajectories. To address this, we propose Plan-Verify-Fill (PVF), a training-free paradigm that grounds planning via quantitative validation. PVF actively constructs a hierarchical skeleton by prioritizing high-leverage semantic anchors and employs a verification protocol to operationalize pragmatic structural stopping where further deliberation yields diminishing returns. Extensive evaluations on LLaDA-8B-Instruct and Dream-7B-Instruct demonstrate that PVF reduces the Number of Function Evaluations (NFE) by up to 65% compared to confidence-based parallel decoding across benchmark datasets, unlocking superior efficiency without compromising accuracy.

## 1. Introduction

DLMs (Gong et al., 2024; Shi et al., 2024; Lou et al., 2024; Ye et al., 2025a; Nie et al., 2025) extend the iterative denoising paradigm of diffusion models to discrete text generation, offering an alternative to the strictly sequential decoding employed by AR models. By operating over a global canvas and iteratively refining token predictions, DLMs unlock substantial potential for parallel token updates. This global representation further enables reasoning over long-range structure and planning dependencies across the sequence (Li et al., 2022). Recent studies, together with real-world deployments (Khanna et al., 2025; Nie et al., 2025; Ye et al.,

2025a; Google DeepMind, 2025), demonstrate that masked diffusion architectures scale well and deliver competitive performance across a range of tasks.

This same flexibility also introduces new challenges. By relaxing the strict left-to-right decoding constraint, DLMs expand the space of admissible decoding orders, with autoregressive generation emerging as a special case within this broader framework. From this perspective, mask-based diffusion models can be interpreted as AR models operating under unconstrained generation orders (Hoogeboom et al., 2021). This enlarged space of decoding trajectories offers the potential to discover generation orders that better align with task structure, but it also includes many trajectories that are poorly matched to the natural sequential organization of language. This gap highlights a fundamental challenge of diffusion-based generation: approaching the theoretical potential of diffusion decoding by identifying trajectories that are both reliable and capable of fully leveraging parallel execution.

In practice, many existing decoding strategies address this challenge conservatively, despite the fact that the strategic potential of the global canvas in DLMs extends beyond simply harvesting the model’s most immediate predictions. Current confidence-based strategies focus on securing “safest bets”, locking in tokens as soon as they reach a high-probability threshold (Gong et al., 2024; Chang et al., 2022; Ye et al., 2025a; Wu et al., 2025b). While this heuristic efficiently resolves local syntax, it adopts a passive stance toward global structure, effectively waiting for complex dependencies to emerge rather than actively planning them. Consequently, the decoding process risks settling for the path of least resistance, failing to fully leverage the diffusion framework’s unique capacity to actively coordinate long-range decisions across the sequence.

To overcome this limitation, a promising avenue is to design decoding strategies that explicitly leverage the intrinsic structural foresight of underlying language models (LMs). Emerging evidence suggests that semantic construction in LMs is not a uniform flow, but rather a rhythmic process punctuated by sparse, high-leverage decision points that shape global generation trajectories. Mechanistic interpreta-

<sup>1</sup>Department of Georgia Institute of Technology, Georgia Institute of Technology, Atlanta, USA <sup>2</sup>University of California, Berkeley, USA. Correspondence to: Miao Li <mli746@gatech.edu>, Hanyang Jiang <scottjhy@gatech.edu>.

tions substantiate this view: [Li et al. \(2025b\)](#) demonstrates that attention dynamics encode a “mechanistic blueprint” of reasoning roles, rendering the model’s internal logic legible not merely as a byproduct of computation. Complementing this, [Men et al. \(2024\)](#) argues that planning is not an external add-on; rather than generating tokens in a purely reactive manner, models appear to internally encode short-horizon plans.

Recent work suggests that planning-related signals may be associated with a subset of high-leverage tokens that correlate with downstream reasoning structure and trajectory ([Zhang et al., 2023](#); [Bogdan et al., 2025](#); [Ye et al., 2025b](#); [Wang et al., 2023](#); [Zhou et al., 2025](#)). By treating discourse scaffolds, such as formatting markers, as discrete control variables, we can explicitly lock in the step-wise logical skeleton before expending computation on fine-grained lexical details.

Therefore, we propose **Plan-Verify-Fill (PVF)** to operationalize active structural steering within the decoding process. PVF (see Figure 1 for an overview) employs a dual-route architecture to decouple high-level skeleton generation from fine-grained filling. The **Planning Route** proactively injects “planning tokens” to guide the global trajectory, while a rigorous **Verification Mechanism**—based on the *impact set*—ensures these “bold” structural commitments remain mathematically consistent with the model’s latent consensus. When structural planning yields diminishing returns, an **AR Fallback Route** executes dense content resolution. Recognizing the limits of abstract planning, this mechanism rapidly populates blank spaces to stabilize the immediate context, thereby revealing the latent structural outline via bottom-up execution. Together, these components enable planning-aware decoding without sacrificing robustness.

Empirically, our analysis suggests that actively regulating the planning horizon leads to superior decoding efficiency. We evaluate PVF across six diverse benchmarks, including GSM8K, MMLU-Pro, ARC-C, WinoGrande, HumanEval, and Math, using LLaDA-8B-Instruct and Dream-7B-Instruct to demonstrate model-agnostic robustness. By proactively securing high-leverage anchors, PVF breaks the bottleneck of passive confidence thresholds, achieving NFE reductions of over 60% on GSM8K, MMLU-Pro, ARC-C and WinoGrande, and over 40% on complex reasoning tasks compared to strong baselines like Fast-dLLM and FreeDave.

Our contributions can be summarized as follows:

- We introduce **PVF**, a training-free parallel decoding strategy that shifts generation from reactive token harvesting to active planning, locking in a hierarchical skeleton via discourse scaffolds before refining local content. To the best of our knowledge, PVF is among

the first approaches to incorporate semantic cues as an explicit decision signal in DLM parallel decoding, surpassing reliance on token probabilities alone.

- A **Consistency Verification** protocol, formalized via impact sets, that enforces validity constraints on all steering decisions, ensuring structural commitments remain mathematically consistent with the model’s latent consensus *without degrading final decoding accuracy*.
- PVF establishes a training-free, model-agnostic paradigm, leveraging batch parallelism to detect structural saturation, and it optimizes the deliberation budget without requiring parameter updates.

## 1.1. Related Work

**Parallel Decoding** The scalability of global denoising has enabled the rise of DLMs ([Nie et al., 2025](#); [Ye et al., 2025a](#); [Zhu et al., 2025](#)), which now rival autoregressive baselines in performance while offering massively parallel inference ([Prabhudesai et al., 2025](#)). To harness this potential, recent studies have explored hybrid block-wise diffusion ([Chen et al., 2024](#); [Arriola et al., 2025](#); [Nie et al., 2025](#)), merging autoregressive flexibility with parallel throughput. Algorithmically, strategies have evolved from rigid schedules ([Chang et al., 2022](#)) to adaptive strategies ([Yu et al., 2025](#); [Wu et al., 2025b](#); [Fu et al., 2025](#); [Ben-Hamu et al., 2025](#); [Wu & Zhang, 2025](#)) that leverage position-specific calibration, uncertainty-driven exploration, and verification protocols to minimize decoding steps.

**Planning Tokens** Recent investigations reveal that the locus of planning is intrinsically tied to discrete semantic units. [Zhang et al. \(2023\)](#) utilizes math operation tokens to abstract macro-level logic, effectively decoupling mathematical strategies from natural-language explanations. Similarly, [Bogdan et al. \(2025\)](#) identifies high-leverage components as “Thought Anchors”—sparse linguistic triggers that actively steer the global reasoning trajectory. Expanding on this hierarchical view, both [Wang et al. \(2023\)](#) and [Zhou et al. \(2025\)](#) demonstrate that self-defined special tokens can be trained to encapsulate the semantic essence of planning, serving as a self-defined map for the generation process. [Ye et al. \(2025b\)](#) demonstrates that structural markers and formatting constraints possess distinct learning dynamics, being significantly more predictable than instance-specific reasoning content. Inspired by this distinction, we operationalize these repetitive structural scaffolds as stable cognitive anchors in PVF, offering a low-uncertainty foundation upon which more volatile semantic reasoning can be safely constructed.

**Hierarchy-aware decoding for DLMs** In this work, we classify strategies that separate structural planning from

content realization as hierarchical-structure-aware decoding. This paradigm has evolved from early latent refinement methods (Li et al., 2022) to explicit separations, such as the semantic scales (Zhou et al., 2025) and the planner–executor framework of Berrayana et al. (2025), designed to isolate intermediate planning from the distinct phase of final answer generation. Most relevant to our approach are Israel et al. (2025), utilizing an autoregressive phase to lock in structural control tags, and Li et al. (2025a), which identifies structural chunks via data-driven confidence thresholds. PVF distinguishes itself by synergizing semantic intent with statistical rigor. Unlike the static, upfront commitments of Israel et al. (2025), PVF adopts an iterative approach that evolves the structural plan as the context matures, effectively reducing the reliance on precise upfront planning. Furthermore, in contrast to the purely statistical proxies of Li et al. (2025a), PVF employs a dual certification protocol: anchors must be both semantically significant and statistically stable. This allows PVF to detect the exact point of structural saturation, while remaining a lightweight, training-free solution that avoids the retraining overhead of prior studies.

## 2. Preliminary

Departing from the left-to-right decoding of AR models, DLMs (Austin et al., 2021; Lou et al., 2023; Ou et al., 2024) recast generation as an iterative refinement task. This framework adapts diffusion principles to the discrete domain via two governing dynamics: a forward process that systematically corrupts the sequence by masking tokens, and a parameterized reverse process trained to recover the original text from the corrupted state.

**Forward Process (Corruption):** The forward process  $q(\mathbf{x}_s | \mathbf{x}_0)$  defines a transition distribution that progressively corrupts the clean data vector  $\mathbf{x}_0$  over a continuous time horizon  $s \in [0, 1]$ . In this framework, tokens are replaced by a special mask token `[MASK]`, which serves as an *absorbing state*—once a token becomes masked, it remains masked throughout the process. Consequently, the clean sequence  $\mathbf{x}_0$  is gradually transformed into a fully masked sequence at  $\mathbf{x}_1$ . In other words, this process is defined by the transition probability, following the notation in (Austin et al., 2021):

$$\begin{aligned} q(\mathbf{x}_s | \mathbf{x}_0) &= \prod_{i=1}^{|\mathbf{x}_0|} q(x_s^i | x_0^i) \\ &= \prod_{i=1}^{|\mathbf{x}_0|} \text{Cat}\left(x_s^i; (1-s)\delta_{x_0^i} + s\delta_{[\text{MASK}]}\right). \end{aligned}$$

**Reverse Process (Denoising):** Given an input sequence  $\mathbf{y} = [\mathbf{y}_{\text{prompt}}, \mathbf{y}_{\text{gen}}]$ , where  $\mathbf{y}_{\text{prompt}}$  denotes the fixed context and  $\mathbf{y}_{\text{gen}} \in \mathcal{V}^L$  represents the masked sequence to be gen-

erated over a vocabulary  $\mathcal{V}$ . The generation model  $P_\theta$  is commonly trained under an ELBO-based objective (Nie et al., 2025; Sahoo et al., 2024; Ou et al., 2024), to recover clean data from corrupted states. During inference, generation proceeds by iteratively reversing the forward corruption process using the learned transition  $P_\theta(\cdot | \mathbf{y}_t)$ . At each timestep  $t$  during inference, the fitted model  $P_\theta$  produces a more refined estimate of the underlying clean sequence from the noisy state

$$\mathbf{y}_t = [y_t^1, \dots, y_t^L] \in \mathcal{V}^L,$$

where each token representation  $y_t^i$  corresponds to a categorical distribution over the vocabulary  $\mathcal{V}$ .

**Confidence-based Parallel Decoding:** One of the most prominent decoding strategies in DLMs is confidence-based decoding (Yu et al., 2025), which governs the generation process based on prediction certainty.

For each currently masked position  $i$  at step  $t$ , we define the model’s top prediction  $\hat{y}_t^i$  conditioned on the state from the previous step  $\mathbf{y}_{t-1}$ :

$$\hat{y}_t^i = \arg \max_{w \in \mathcal{V}} P_\theta(y^i = w | \mathbf{y}_{t-1}).$$

In its most canonical form, the algorithm progressively fills the sequence by committing to tokens where the model’s confidence exceeds a static threshold  $\tau_{\text{high}}$ . The update rule is given by:

$$y_t^i = \begin{cases} \hat{y}_t^i, & \text{if } P_\theta(y^i = \hat{y}_t^i | \mathbf{y}_{t-1}) \geq \tau_{\text{high}}, \\ y_{t-1}^i, & \text{otherwise.} \end{cases} \quad (1)$$

While this static heuristic serves as a basic building block for parallel decoding, later approaches (Wu et al., 2025b; Fu et al., 2025; Chen et al., 2025; Jin et al., 2025; Lou et al., 2024) adopt more complex decoding mechanisms that extend beyond heuristic gating, enabling adaptive control over diffusion steps for efficient parallel generation.

**Semi-Autoregressive Blockwise Decoding** Semi-AR diffusion adopts a hybrid structure combining *inter-block* autoregression with *intra-block* parallel diffusion. Widely adopted in modern DLMs (Arriola et al., 2025; Ye et al., 2025a; Nie et al., 2025; Sahoo et al., 2024; Wu et al., 2025a;b), this strategy restricts attention to local regions, thereby reducing inference cost while preserving the local context often lost in fully parallel approaches. First partition the fixed canvas length  $L$  into  $B$  blocks, writing

$$\mathbf{y}_t = [y_t^{1:L/b}, y_t^{L/b+1:2(L/b)}, \dots, y_t^{L-b+1:L}].$$

The  $k$ -th block encompasses the token segment spanning from index  $(k-1)\frac{L}{B} + 1$  to  $k\frac{L}{B}$ . During inference, the

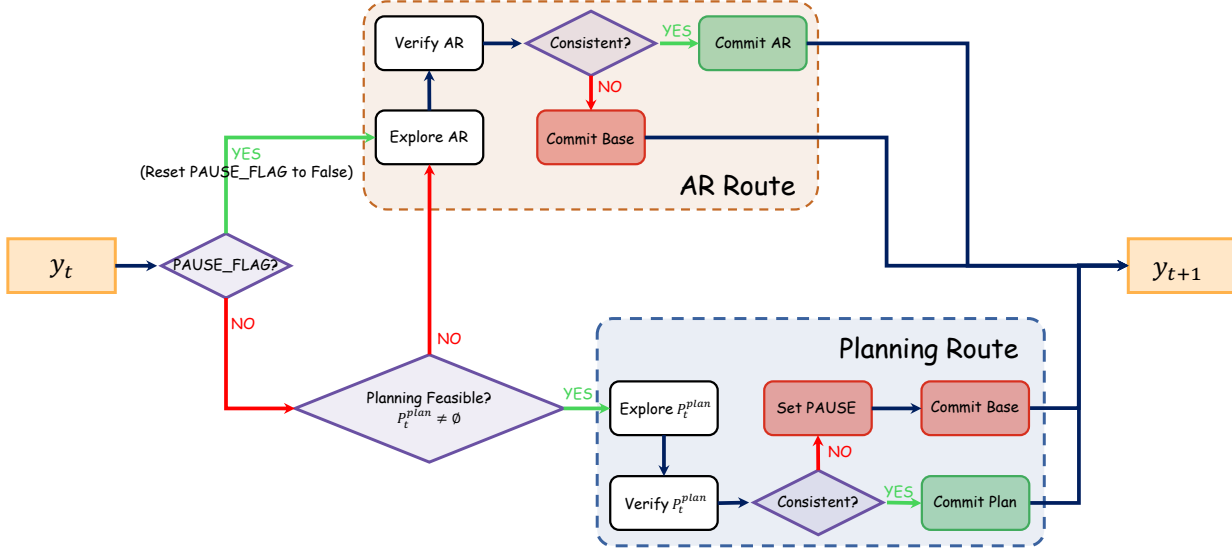


Figure 1. Overview of the Plan–Verify–Fill (PVF) decoding pipeline.

decoding process adheres to a block-causal constraint: the state  $y_t$  can commit tokens in the  $(k + 1)$ -th block only if the  $k$ -th block is fully resolved (i.e., contains no [MASK] tokens); otherwise, all subsequent blocks  $j > k$  must remain strictly masked.

We define  $\mathcal{B}_t$  to represent the set of indices for the current *working block(s)* where [MASK] tokens are eligible for replacement at step  $t$ .

For example, in a strictly semi-autoregressive block diffusion setting, if the first block (indices 1 to  $L/B$ ) is fully unmasked while the second block remains incomplete,

$$\mathcal{B}_t = \{i \mid y_t^i = [\text{MASK}]\} \cap \left\{ \frac{L}{B} + 1, \dots, \frac{2L}{B} \right\}.$$

### 3. Inducing Hierarchical Structure with Planning Tokens

Prior work shows that adaptively lowering the confidence threshold can substantially accelerate diffusion decoding with limited accuracy loss (Wu et al., 2025b). This raises a natural question: *Are all lower-confidence tokens, based primarily on a probabilistic threshold, equally safe to commit, or are some intrinsically safer to decode early? For example, when multiple candidates fall within the same low-confidence band near the threshold, does the specific choice among them matter?*

This question is especially salient for DLMs because decoding requires navigating an enormous search space: unlike AR models that collapse uncertainty sequentially, DLMs must jointly resolve both *what* to say (content generation) and *how* to organize it (structural planning) across a global canvas. To answer this question, we examine token-

level confidence dynamics and find empirically that low-confidence tokens vary substantially in reliability: *planning tokens*, a small set of structurally salient anchors, can often be committed early at lower confidence with noticeably smaller degradation in accuracy.

**The Safety of Content-Neutral Anchors.** A natural concern with forcing low-confidence tokens is the risk of “hallucination” or error propagation. Here, we distinguish between *Content Risk* and *Structural Risk*.

- **Content Forcing (High Risk):** Forcing a dense content token (e.g., a specific number like “7” or a variable name) when confidence is low is dangerous. If the model is unsure, forcing a specific value creates a factual premise that may lead to an instant, unrecoverable error.
- **Structure Forcing (Low Risk):** In contrast, Planning Tokens are largely *content-neutral*. Forcing a logical connector like “Therefore” does not assert a fact; instead, it mainly imposes a *topological constraint*.

**Restricting Search Space via Structural Constraints.** Content generation is inherently instance-specific, so many fine-grained details are difficult to settle early in decoding. Structural cues, in contrast, are far more consistent across instances (e.g., in code, tokens like `def`, `return`, and `main` recur broadly), motivating us to examine whether they can be committed earlier. This asymmetry is important because low confidence does not necessarily reflect missing knowledge: it could arise from *trajectory ambiguity*, where probability mass is split across competing trajectories, and certainty consolidates slowly.

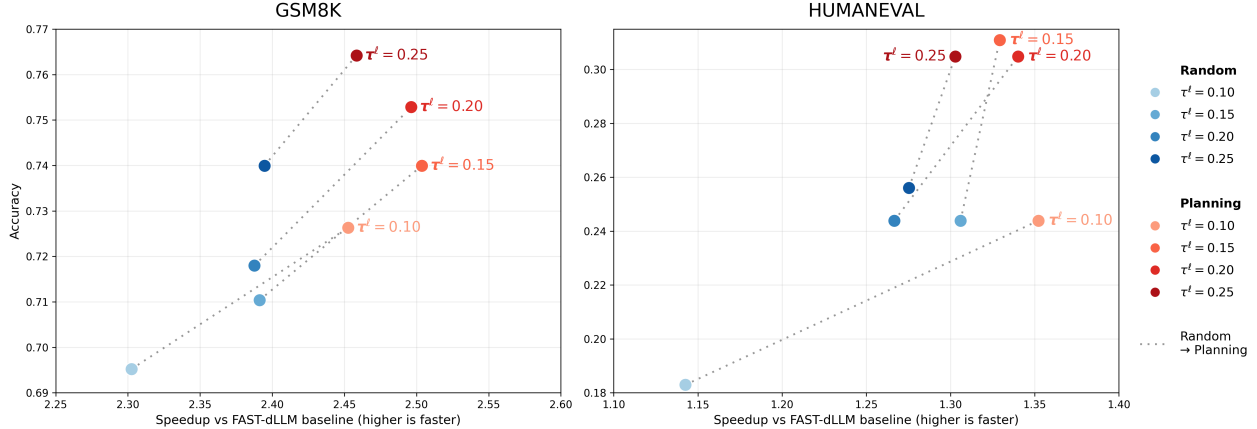


Figure 2. Ablation on GSM8K and HumanEval comparing lower-confidence commits of planning tokens versus random tokens (i.e., without prioritizing planning tokens). Across confidence bins, prioritizing planning tokens consistently yields faster decoding and improved accuracy; points closer to the upper-right indicate better performance on both axes.

We leverage this asymmetry to explore a simple intervention: prioritizing the commitment of *Planning Tokens*, a specialized subset of the vocabulary  $\mathcal{P}$  (e.g., logical connectors such as `Therefore` and structural separators; see Sections 3.1 and A.1), to prune the search space. We hypothesize that such early structural commitments may help disambiguate competing trajectories and guide the model toward a coherent structural skeleton.

Empirically, we adopt the static variant of Fast-dLLM (Wu et al., 2025b) as the baseline. At each decoding step, in addition to the tokens selected by Fast-dLLM, we randomly commit one extra token whose confidence lies within a prescribed low-confidence interval  $[\tau^l, \tau^u]$ . In Figure 2, we fix  $\tau^u = 0.6$  for simplicity. The results show that unrestricted low-confidence commitments (labeled *Random* in Figure 2) cause substantial performance degradation, whereas prioritizing our content-neutral planning token set  $\mathcal{P}$  for such commitments (labeled *Planning* in Figure 2) markedly reduces the accuracy loss while also improving efficiency. Additional experimental details are provided in Section A.2.

### 3.1. Automated Discovery via Structural Distillation

Manually constructing a comprehensive planning vocabulary  $\mathcal{P}$  is intractable given the diversity of generation contexts. To address this, we utilize a modern LLM as a *structural distillation engine* to extract a compact set of *domain-invariant* tokens that serve as reusable reasoning scaffolds. Concretely, we prompt the model to identify a “structural skeleton” of valid syntax that satisfies the following criteria:

1. **High Structural Leverage:** tokens that act as frequent control anchors (e.g., logical connectives, syntactic delimiters, or control-flow keywords) and meaningfully constrain the global structure of the generation;

2. **Content Neutrality:** tokens that are agnostic to specific instances, avoiding dense semantic content (e.g., numerical constants) while expressing relations or structure.

Additional implementation and prompt details are provided in Section A.1.

## 4. Methodology: Plan-Verify-Fill (PVF) Decoding

Building upon the above findings, we propose **Plan-Verify-Fill (PVF)**, a novel decoding strategy for Diffusion Language Models that leverages *planning tokens* to guide generation. In addition to parallel decoding, PVF alternates between committing high-level structural anchors via planning and applying an accelerated AR fallback to accelerate fine-grained completion. By decoupling structural generation from local content filling, this approach ensures that detailed tokens are decoded only after the global context is stable, thereby minimizing premature commitments in high-uncertainty regions. By exploiting batch parallelism, this evaluation incurs negligible latency.

**Overview of the PVF Pipeline** The PVF process operates via a dual-route architecture. The primary **Planning Route** proceeds in two phases: (1) **Proposal**, where planning tokens are tentatively injected based on a lower confidence threshold  $\tau_{\text{plan}}$  to encourage structural buildup; and (2) **Verification**, which enforces consistency with high-confidence parallel-decoding decisions under  $\tau_{\text{high}}$ . Should this route fail, the system reverts to the **AR Fallback Route**, a secondary mechanism that bypasses planning and advances decoding via local filling with a route-specific consistency check, when planning cues are insufficient (see Figure 1).

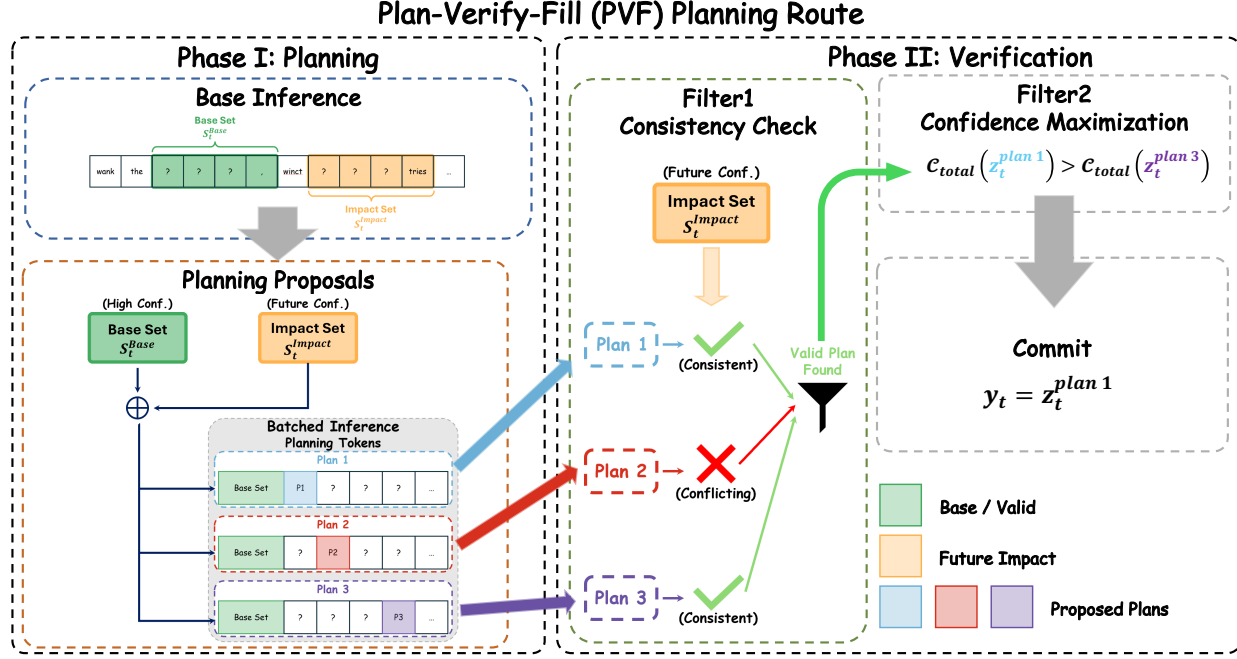


Figure 3. Overview of the Planning Route

**Safeguarding Consistency through the Impact Set**  
 While recent work shows that exploiting lower-confidence tokens is key for decoding efficiency (Fu et al., 2025; Wu & Zhang, 2025; Wu et al., 2025b; Huang et al., 2025), such commits are not uniformly safe: in some cases, a suboptimal early commitment can bias the trajectory away from valid semantic attractors. PVF addresses this risk through a verification mechanism that validates each tentative commit by checking its downstream consistency over the affected positions under a route-specific criterion.

To formalize this safety constraint, we define the *impact set*  $S_{\text{impact}}$ . Let  $\mathcal{M}(\mathbf{y}) = \{i \in \mathcal{B}_t \mid y^i = [\text{MASK}]\}$  denote the set of indices within the current target block  $\mathcal{B}_t$  that remain masked in state  $\mathbf{y}$ . For simplicity, we denote the masked set at step  $t$  as  $\mathcal{M}_t = \mathcal{M}(\mathbf{y}_t)$ . Given a target criteria set  $S$ , the impact set is defined as

$$S_{\text{impact}}(\mathbf{y}, S) = \mathcal{M}(\mathbf{y}) \cap S \quad (2)$$

In our evaluation, we use  $S = S_{\text{high conf}}(\mathbf{y}) = \{i \in \mathcal{B}_t \mid \hat{y}^i \geq \tau_{\text{high}}\}$ , which represents the subset of masked indices where the model is confident enough to form a “visible” future context. By monitoring  $S_{\text{impact}}$  as a validity verifier, we impose a consistency constraint so that additional commits remain aligned with the parallel-decoding criterion induced by  $\tau_{\text{high}}$ : a valid plan must preserve (or expand) the set of high-confidence future tokens established by the baseline. This metric serves as a safeguard, ensuring that bold decoding unlocks new information without destabilizing the model’s global trajectory.

At decoding step  $t$ , with previously committed state  $\mathbf{y}_{t-1}$  and mask index set after the previous commit  $\mathcal{M}_{t-1}$ , we first identify the **Base Set** of high-confidence tokens:

$$S_t^{\text{base}} = \{i \in \mathcal{M}_{t-1} \mid \hat{y}_t^i \geq \tau_{\text{high}}\} \quad (3)$$

Committing the tokens in  $S_t^{\text{base}}$  yields the intermediate *base state*  $\mathbf{z}_t^{\text{base}}$ :

$$z_t^{i, \text{base}} = \begin{cases} \hat{y}_t^i, & i \in S_t^{\text{base}} \\ y_{t-1}^i, & i \in [L] \setminus S_t^{\text{base}} \end{cases} \quad (4)$$

Intuitively,  $S_{\text{impact}}(\mathbf{z}_t^{\text{base}}, S_{\text{high conf}})$  captures the “future” tokens revealed by these base commitments.

#### 4.1. Planning Route Phase I: Planning Proposal

Recent studies indicate that on modern accelerators, inference latency for small batch sizes (e.g., 1 vs. 4) is virtually identical due to memory bandwidth saturation (Wu & Zhang, 2025; Fu et al., 2025). We exploit this parallelism to verify multiple planning candidates simultaneously alongside the baseline trajectory (see Figure 3).

**Planning Token Candidates** Simultaneously, we identify candidate positions for planning. Given the vocabulary of planning tokens  $\mathcal{P}_{\text{plan}}$ , we construct the candidate set  $\mathcal{P}_t^{\text{plan}}$  based on  $\mathcal{P}_{\text{plan}}$  at step  $t$  by identifying masked indices where the model predicts a planning token within the reliable confidence interval  $[\tau_{\text{plan}}^l, \tau_{\text{plan}}^u]$ . The lower bound  $\tau_{\text{plan}}^l$  acts as a reliability floor, explicitly filtering out low-confidence

predictions that would otherwise introduce instability into the generation trajectory. The upper bound  $\tau_{\text{plan}}^u$  serves as an efficiency constraint, excluding tokens that are already approaching convergence (i.e., nearing  $\tau_{\text{high}}$ ). When the model’s confidence exceeds this threshold, the probability distribution is highly peaked, meaning the search space of potential trajectories is *already* effectively pruned. Triggering a dedicated planning mechanism in this regime is computationally redundant, as it yields diminishing returns in further reducing uncertainty. Instead, we target the “ambiguous but promising” interval—tokens where the model exhibits strong intuition but lacks finality—ensuring that the expensive planning budget is allocated strictly to critical decision points where lookahead can significantly clarify the trajectory:

$$\mathcal{P}_t^{\text{plan}} = \left\{ i \in \mathcal{M}_{t-1} \mid \hat{y}_t^i \in \mathcal{P}_{\text{plan}} \wedge \tau_{\text{plan}}^l \leq P_\theta(y^i = \hat{y}_t^i \mid \mathbf{y}_{t-1}) < \tau_{\text{plan}}^u \right\} \quad (5)$$

We then create an ordered sequence of indices from the candidate set  $\mathcal{P}_t^{\text{plan}}$  by sorting them based on the trained model  $P_\theta$ ’s prediction confidence. Let  $i_{(j)}$  denote the index of the  $j$ -th most confident candidate, such that:

$$P_\theta(y^{i_{(1)}} = \hat{y}_t^{i_{(1)}} \mid \mathbf{y}_{t-1}) \geq P_\theta(y^{i_{(2)}} = \hat{y}_t^{i_{(2)}} \mid \mathbf{y}_{t-1}) \geq \dots \quad (6)$$

where  $\hat{y}_t^{i_{(k)}}$  is the predicted token at position  $i_{(k)}$ . We select the top- $k$  candidates ( $j \in \{[k]\}$ ) to construct the planned trajectories

$$z_t^{i_{\text{plan}}, j} = \begin{cases} \hat{y}_t^i, & i = i_j \\ z_t^{i_{\text{base}}}, & \text{otherwise} \end{cases} \quad (7)$$

Based on a recent paper (Wu et al., 2025b), there is a “free lunch” region where the batch inference costs almost the same computational time as a single sample. Empirical verification (Fu et al., 2025) demonstrates that on the B200, the forward-pass latency for a batch size of 4 is effectively identical to that of a single sample. Leveraging this observation, we set  $k = 3$ . This configuration allows us to evaluate three planned candidates alongside the single baseline trajectory (a total batch size of 4), maximizing structural exploration without incurring any runtime penalty. Finally, the control flow adapts to candidate availability. If  $\mathcal{P}_t^{\text{plan}} = \emptyset$ , it indicates that the current context requires local infilling to establish a sufficient foundation before structural planning can resume. In this scenario, we bypass Phase II and pivot directly to the AR Fallback Route. Conversely, if valid candidates exist but are sparse ( $1 \leq |\mathcal{P}_t^{\text{plan}}| < 3$ ), we construct trajectories using all available indices and proceed to Phase II.

## 4.2. Planning Route Phase II: Verification (The Two-Filter Mechanism)

The design of PVF explicitly distinguishes between *guiding* the model toward coherent structures and *forcing* it into suboptimal commitments. To operationalize this distinction, we employ a two-filter mechanism that rigorously assesses the validity of the planned trajectories generated in Phase I.

**Filter 1: Consistency Verification.** A planning token is deemed premature if committing to it forces a contradiction in the high-impact future tokens  $\mathcal{S}_{\text{impact}}$  inferred from the base state. Specifically, for each planned trajectory  $j$ , we verify  $\forall i \in \mathcal{S}_{\text{impact}}(\mathbf{z}_t^{\text{base}}, S_{\text{high conf}}(\mathbf{z}_t^{\text{base}}))$  if:

$$\arg \max_{w \in \mathcal{V}} P_\theta(y^i = w \mid \mathbf{z}_t^{\text{base}}) = \arg \max_{w \in \mathcal{V}} P_\theta(y^i = w \mid \mathbf{z}_t^{\text{plan}, j}) \quad (8)$$

In other words, while the probability distributions over the impact set are permitted to fluctuate, the top-1 predictions must remain strictly invariant relative to the Base branch. If a planning token induces a label flip within this high-confidence future region, the candidate trajectory is rejected. This constraint guarantees that introducing planning tokens does not induce behavior inconsistent with the stable consensus established by the model’s highest-confidence predictions.

Should no candidates satisfy Filter 1, the **PAUSE** mechanism is triggered to prevent cascading errors (i.e `PAUSE_FLAG` is set to `True`). This failure signal indicates that the proposed planning steps are too aggressive given the current uncertainty; the model lacks sufficient context to reliably establish long-range structure. Consequently, the decoding priority shifts from structural expansion to dense content resolution—filling in the necessary semantic details required to stabilize the context before resuming planning. This mechanism temporarily disables planning, forces a reversion to AR Filling, and commits the base trajectory  $\mathbf{y}_t = \mathbf{z}_t^{\text{base}}$  for the current step.

**Filter 2: Confidence Maximization.** Among the candidates  $\mathbf{z}_t^{\text{plan}, j}$  that pass Filter 1, we define the *Total Confidence Score* within the current block  $\mathcal{B}_t$ :

$$\mathcal{C}_{\text{total}}(\mathbf{z}_t^{\text{plan}, j}) = \sum_{i \in \mathcal{B}_t \cap \mathcal{M}(\mathbf{z}_t^{\text{plan}, j})} \max_{w \in \mathcal{V}} P_\theta(y^i = w \mid \mathbf{z}_t^{\text{plan}, j}) \quad (9)$$

We commit the trajectory  $\mathbf{z}_t^{\text{plan}, j^*}$  that yields the largest  $\mathcal{C}_{\text{total}}$ , i.e  $\mathbf{y}_t = \mathbf{z}_t^{\text{plan}, j^*}$ . Maximizing this metric implies that the selected planning token provides the optimal structural conditioning, thereby maximizing the semantic resolution of the surrounding tokens and allowing the model to fill the local context with the highest certainty.

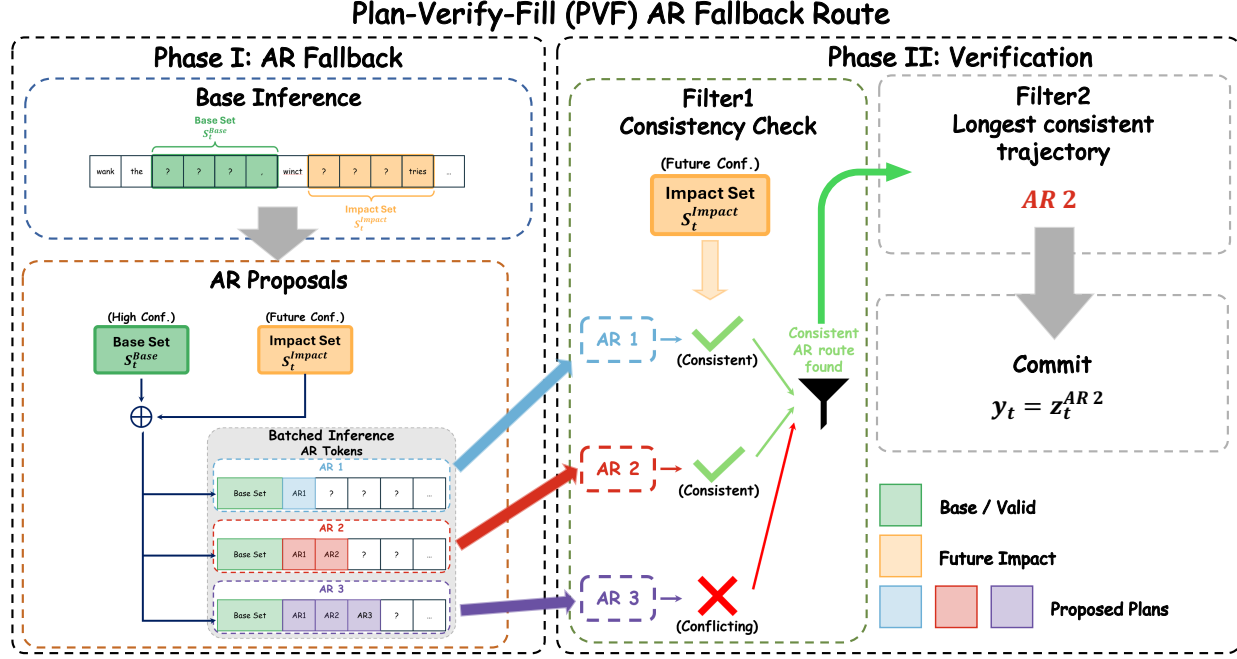


Figure 4. Overview of the AR Fallback Route

#### 4.3. AR Route: Autoregressive Fallback with Verification

If the planning route is unavailable or paused, we utilize **Autoregressive (AR) Filling** to accelerate local content completion before structural planning resumes (see Figure 4). This phase operates as a speculative generation mechanism designed to efficiently fill local content before the next structural planning step.

**Candidate Construction.** A batch of candidate trajectories is constructed by tentatively fixing the  $k$ -leftmost masked tokens (for  $k = 1, 2, 3$ ) from the set  $\mathcal{M}_{t-1} \setminus S_t^{\text{base}}$ . Let these indices be denoted as  $\{i_1^{\text{AR}}, i_2^{\text{AR}}, i_3^{\text{AR}}\}$  in ascending order. The AR candidate trajectories  $z_t^{\text{AR}, k}$  are defined as follows:

$$z_t^{\text{AR}, k} = \begin{cases} \hat{y}_t^i, & i \in \{i_1^{\text{AR}}, \dots, i_k^{\text{AR}}\} \\ z_t^{\text{base}}, & \text{otherwise} \end{cases} \quad (10)$$

where  $\hat{y}_t^i$  corresponds to the prediction from the initial base forward pass.

**Training-Free Speculative Decoding.** This design implements an adaptive form of speculative decoding. Unlike classical speculative decoding in AR models, approaches that require training a separate student model or draft head (Leviathan et al., 2023), we project this paradigm as a purely inference-time procedure. By using greedy prefixes of the base model’s own predictions as “drafts,” our method is training-free, unaffected by distribution shifts in student

models, and immediately applicable to any off-the-shelf DLM backbone.

**AR Verification.** To ensure generation quality, we design a rigorous verification process. We accept a  $k$ -token extension only if the model’s predictions on the new trajectory are *consistent* with the tentative drafts. Formally, for a candidate  $k$ , we verify:

$$\begin{aligned} \forall i \in \{i_1^{\text{AR}}, \dots, i_k^{\text{AR}}\}, \\ \text{argmax}_{w \in \mathcal{V}} P_{\theta}(y^i = w \mid z_t^{\text{base}}) = z_t^{i, \text{AR}, k} \end{aligned} \quad (11)$$

Let  $k^*$  denote the largest  $k$  satisfying the verification condition (11). We commit the corresponding trajectory  $y_t = z_t^{\text{AR}, k^*}$ . This constraint ensures that the AR fallback only accepts tokens that remain stable under the updated context, effectively mitigating hallucinations.

In the event that no candidate passes verification, the system reverts to the base state  $y_t = z_t^{\text{base}}$ . Upon entering the AR fallback phase, the PAUSE\_FLAG is reset to False. This ensures the suspension of planning is transient, encouraging the model to re-attempt structural planning in subsequent steps once the local context has been stabilized.

#### 4.4. Planning-Guided Early Cross-Block Revelation

While retaining block-wise efficiency, we discard the rigid constraint of strictly sequential convergence. Our motivation is structural: as the active block enters a *saturated regime* of mask scarcity, the constricted search space limits



Figure 5. Ablation study on the full GSM8k dataset evaluating the contribution of each PVF component. Accuracy scores are displayed above each bar to confirm they remain comparable across methods.

the planner’s optimization capacity. To counteract this, we adopt a *dynamic expansion strategy* that reveals the subsequent block preemptively when the current block’s sparsity hinders effective planning.

Consistent with recent approaches that relax rigid block boundaries (Wang et al., 2025; Fu et al., 2025), we allow for early cross-block revelation to facilitate information flow. However, to mitigate the accuracy degradation often observed with aggressive expansion (Wang et al., 2025), this strategy is implemented conservatively. Expansion is only triggered when the current block enters a saturated regime of mask scarcity, ensuring that the early decoding mechanism serves solely to maintain a valid planning horizon.

Formally, the block size is denoted as  $S = L/B$ . We identify the index of the current active block  $k_t$  as the first block containing masked tokens. Define the index set of masked tokens in the current active block  $\mathcal{M}_{t-1}^{\text{active}} = \mathcal{M}_{t-1} \cap \{S(k_t - 1) + 1, \dots, Sk_t\}$ . We define the working index set  $\mathcal{B}_t$  by checking if the remaining masks in the current block fall below a sparsity threshold  $N_s$ :

$$\mathcal{B}_t = \begin{cases} \mathcal{M}_{t-1}^{\text{active}} \cup \mathcal{I}_{k_t+1}, & \text{if } |\mathcal{M}_{t-1}^{\text{active}}| \leq N_s \\ \mathcal{M}_{t-1}^{\text{active}}, & \text{otherwise} \end{cases} \quad (12)$$

where  $\mathcal{I}_{k_t+1} = \{k_t S + 1, \dots, (k_t + 1)S\}$  represents the full index range of the next block. This condition ensures that the planner always operates on a sufficiently broad horizon, seamlessly transitioning focus to  $k + 1$  as block  $k_t$  stabilizes.

## 5. Experiment Results

### 5.1. Experiment Settings

We evaluate both generation quality and decoding efficiency of our proposed PVF strategy on six benchmark datasets spanning mathematical reasoning, coding synthesis, and broad knowledge: GSM8K (Cobbe et al., 2021), MMLU-

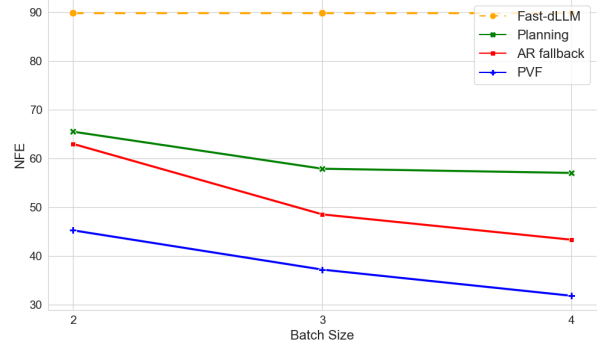


Figure 6. Ablation study on the full GSM8k dataset evaluating the impact of PVF components across varying batch sizes in the “free lunch” regime. All results maintain lossless accuracy compared to static decoding.

Pro (Wang et al., 2024), ARC-Challenge (ARC-C) (Clark et al., 2018), WinoGrande (Sakaguchi et al., 2021), HumanEval (Chen et al., 2021), and MATH (Hendrycks et al., 2021). These tasks exhibit distinct output structures—from chain-of-thought reasoning (GSM8K) and multiple-choice knowledge tasks (MMLU-Pro, ARC-C, WinoGrande) to syntax-sensitive programs (HumanEval) and long-form symbolic derivations (MATH)—making them a representative testbed for structure-aware parallel decoding.

We validate PVF’s versatility by benchmarking it on two foundational DLMs, LLaDA-8B-Instruct and Dream-7B-Instruct, and verify that its performance gains are model-agnostic. Across all datasets, we use a fixed maximum generation length of  $L = 512$  and a block size of  $B = 64$ . We perform training-free decoding (no finetuning, no additional supervision, and no external verifier). To ensure a fair comparison, we fix the confidence threshold at  $\tau_{\text{high}} = 0.9$  across all experiments, unless stated otherwise. All experiments are conducted on a single NVIDIA H200 GPU.

**Implementation details.** All methods share the same prompt templates per dataset, the same stopping criterion, and the same maximum generation length. For HumanEval, we follow the standard unit-test protocol and report pass@1; for MATH and GSM8K, we follow exact-match evaluation on the final answer; for MMLU-Pro, ARC-C, and WinoGrande, we report multiple-choice accuracy. Unless otherwise specified, we follow (Fu et al., 2025; Wu & Zhang, 2025) and use a batch size of 4 ( $k = 3$ ), which lies within the “free lunch” region.

### 5.2. Efficiency Metrics

To isolate the algorithmic efficiency of PVF, we measure the Number of Function Evaluations (NFE), the total count of model forward passes required to complete a sequence. We prioritize NFE over throughput metrics like Tokens Per

Table 1. Performance comparison with baseline methods. The model name is listed in the leftmost column, with datasets arranged horizontally.

Model	Method	GSM8K		MMLU-Pro		ARC-C		WinoGrande		HumanEval		Math	
		Acc.	NFE	Acc.	NFE	Acc.	NFE	Acc.	NFE	Acc.	NFE	Acc.	NFE
LLaDA-8B Instruct	Static	79.46	512.00	36.80	512.00	82.46	512.00	70.24	512.00	46.95	512.00	41.06	512.00
	Fast-dLLM	79.62	89.77	36.20	80.26	83.02	48.75	70.24	48.57	47.56	124.26	40.84	147.16
	FreeDave	79.08	135.65	36.70	136.36	84.04	130.73	67.88	131.10	45.73	140.14	40.90	142.82
	PVF	79.62	<b>31.34</b>	36.40	<b>29.55</b>	84.30	<b>17.23</b>	69.93	<b>18.81</b>	48.17	<b>65.26</b>	40.90	<b>80.55</b>
Dream-7B Instruct	Static	78.00	512.00	41.30	512.00	86.95	512.00	70.60	512.00	60.37	512.00	42.20	512.00
	Fast-dLLM	77.71	75.83	40.18	92.16	86.78	56.13	70.65	43.01	59.14	112.78	43.46	129.77
	FreeDave	79.92	141.01	41.10	91.74	88.23	138.91	69.85	134.10	59.15	112.82	42.00	130.25
	PVF	79.20	<b>32.34</b>	43.30	<b>35.22</b>	87.55	<b>25.93</b>	70.81	<b>16.92</b>	62.66	<b>50.89</b>	43.66	<b>64.80</b>

Second (TPS) because NFE provides a hardware-agnostic proxy for computational cost that decouples fundamental algorithmic gains from extrinsic factors such as implementation maturity and system-level optimizations (e.g., kernel fusion). This ensures that reported improvements reflect the intrinsic efficiency of the sampling schedule rather than the optimization state of the research code.

### 5.3. Main Results

**Baselines.** We benchmark PVF against the static decoding and two training-free acceleration frameworks for DLMs that represent complementary design choices: confidence-based parallel commitment and draft-and-verify jumping.

- **Static.** A greedy top-1 decoding strategy that commits the most confident token at each iteration.
- **Fast-dLLM (Wu et al., 2025b).** A static confidence-threshold parallel decoding method that commits all tokens whose posterior confidence exceeds a fixed threshold  $\tau$ .
- **FreeDave (Wu & Zhang, 2025).** A draft-and-verify method that generates multiple look-ahead drafts and accepts the longest consecutively verified jump under top-1 decoding, aiming to match the static trajectory with fewer model forward passes.

**Comparison.** Table 1 summarizes accuracy and NFE across datasets. PVF consistently reduces NFE relative to Fast-dLLM at matched accuracy on all the datasets, while achieving more than 60% fewer forward passes on GSM8K, MMLU-Pro, ARC-C, and WinoGrande, and more than 40% fewer forward passes on MATH and HumanEval. Compared with FreeDave, PVF achieves additional reductions in NFE while maintaining accuracy. Besides, the improvement is consistent across both LLaDa and Dream, indicating the generality of our algorithm. Overall, the results establish PVF as a decoding strategy that delivers substantial efficiency

gains while maintaining accuracy via explicit planning and verification.

**Ablation Study: Contribution of Individual Stages** To quantify the efficiency contribution of each algorithmic component, we decouple the *planning stage* and the *AR fallback stage*. We define the isolated planning stage as committing high-confidence tokens alongside a single verified, lower-confidence planning token, whereas the isolated AR fallback stage commits high-confidence tokens solely via the longest verified AR route. Figure 5 demonstrates that both stages, when applied independently, yield substantial improvements over confidence-based parallel decoding while maintaining accuracy. AR-filling is faster per iteration than planning because it executes at every iteration, whereas planning only activates when a suitable planning token is identified. However, we observe that combining these stages enables PVF to achieve nearly a 30% improvement over AR-filling alone, highlighting the significant efficiency gains provided by the planning mechanism.

**Ablation Study: Sensitivity to Batch Size** To assess whether our algorithm retains efficiency even with more constrained batch sizes, we evaluate the NFE of our PVF method and its individual components as the batch size varies, ensuring that accuracy remains lossless relative to static decoding. In Figure 6, we observe that the planning stage delivers stable performance even at a batch size of 2, whereas the AR fallback benefits more significantly from larger batches due to its cumulative nature. Notably, the full PVF method consistently outperforms both individual components across all settings, and demonstrates substantial efficiency gains compared to the baseline method even at a batch size of 2.

## 6. Conclusion

In this work, we recast the decoding of DLMs not merely as a probabilistic harvesting of tokens, but as a hierarchi-

cal process of structural planning. By introducing **PVF**, we demonstrate that the efficiency of parallel generation is unlocked not only by aggressively predicting content, but by stabilizing the *structural skeleton* of the sequence. Our findings reveal that “planning tokens” are pivotal commits that sharply reduce the search space over global trajectories.

Methodologically, PVF contributes a structured, training-free protocol designed to balance aggressive structural commitment with quantitative verification, reducing inference costs significantly while maintaining comparable accuracy. One potential future direction for DLM decoding is to make the notion of structure more training-aware, so that the model’s representations at inference time better support the same structural decisions PVF makes during decoding. This could better align training and decoding, and may further improve both speed and reliability.

## References

Arriola, M., Gokaslan, A., Chiu, J. T., Yang, Z., Qi, Z., Han, J., Sahoo, S. S., and Kuleshov, V. Block diffusion: Interpolating between autoregressive and diffusion language models. *arXiv preprint arXiv:2503.09573*, 2025.

Austin, J., Johnson, D. D., Ho, J., Tarlow, D., and Van Den Berg, R. Structured denoising diffusion models in discrete state-spaces. *Advances in neural information processing systems*, 34:17981–17993, 2021.

Ben-Hamu, H., Gat, I., Severo, D., Nolte, N., and Karrer, B. Accelerated sampling from masked diffusion models via entropy bounded unmasking. *arXiv preprint arXiv:2505.24857*, 2025.

Berryanya, L., Heakl, A., Sohail, M. A., Hofmann, T., Khan, S., and Chen, W. Planner and executor: Collaboration between discrete diffusion and autoregressive models in reasoning. *arXiv preprint arXiv:2510.15244*, 2025.

Bogdan, P. C., Macar, U., Nanda, N., and Conmy, A. Thought anchors: Which llm reasoning steps matter? *arXiv preprint arXiv:2506.19143*, 2025.

Chang, H., Zhang, H., Jiang, L., Liu, C., and Freeman, W. T. Maskgit: Masked generative image transformer. In *Proceedings of the IEEE/CVF conference on computer vision and pattern recognition*, pp. 11315–11325, 2022.

Chen, B., Martí Monsó, D., Du, Y., Simchowitz, M., Tedrake, R., and Sitzmann, V. Diffusion forcing: Next-token prediction meets full-sequence diffusion. *Advances in Neural Information Processing Systems*, 37:24081–24125, 2024.

Chen, M., Tworek, J., Jun, H., Yuan, Q., Pinto, H. P. d. O., Kaplan, J., Edwards, H., Burda, Y., Joseph, N., Brockman, G., et al. Evaluating large language models trained on code. *arXiv preprint arXiv:2107.03374*, 2021.

Chen, Z., Fang, G., Ma, X., Yu, R., and Wang, X. dparallel: Learnable parallel decoding for dllms. *arXiv preprint arXiv:2509.26488*, 2025.

Clark, P., Cowhey, I., Etzioni, O., Khot, T., Sabharwal, A., Schoenick, C., and Tafjord, O. Think you have solved question answering? try arc, the ai2 reasoning challenge. *arXiv preprint arXiv:1803.05457*, 2018.

Cobbe, K., Kosaraju, V., Bavarian, M., Chen, M., Jun, H., Kaiser, L., Plappert, M., Tworek, J., Hilton, J., Nakano, R., et al. Training verifiers to solve math word problems. *arXiv preprint arXiv:2110.14168*, 2021.

Fu, H., Huang, B., Adams, V., Wang, C., Srinivasan, V., and Jiao, J. From bits to rounds: Parallel decoding with exploration for diffusion language models. *arXiv preprint arXiv:2511.21103*, 2025.

Gong, S., Agarwal, S., Zhang, Y., Ye, J., Zheng, L., Li, M., An, C., Zhao, P., Bi, W., Han, J., et al. Scaling diffusion language models via adaptation from autoregressive models. *arXiv preprint arXiv:2410.17891*, 2024.

Google DeepMind. Gemini diffusion, 2025. URL <https://deepmind.google/models/gemini-diffusion/>. Accessed: 2025.

Hendrycks, D., Burns, C., Kadavath, S., Arora, A., Basart, S., Tang, E., Song, D., and Steinhardt, J. Measuring mathematical problem solving with the math dataset. *arXiv preprint arXiv:2103.03874*, 2021.

Hoogeboom, E., Gritsenko, A. A., Bastings, J., Poole, B., Berg, R. v. d., and Salimans, T. Autoregressive diffusion models. *arXiv preprint arXiv:2110.02037*, 2021.

Huang, P., Liu, S., Liu, Z., Yan, Y., Wang, S., Chen, Z., and Xiao, T. Pcsampler: Position-aware calibration of decoding bias in masked diffusion models. *arXiv preprint arXiv:2508.13021*, 2025.

Israel, D., Jin, T., Cheng, E., Broeck, G. V. d., Grover, A., Subramanian, S., and Carbin, M. Planned diffusion. *arXiv preprint arXiv:2510.18087*, 2025.

Jin, X., Wang, Y., Gao, Y., Wen, Z., Qi, B., Liu, D., and Zhang, L. Thinking inside the mask: In-place prompting in diffusion llms. *arXiv preprint arXiv:2508.10736*, 2025.

Khanna, S., Kharbanda, S., Li, S., Varma, H., Wang, E., Birnbaum, S., Luo, Z., Miraoui, Y., Palrecha, A., Ermon, S., et al. Mercury: Ultra-fast language models based on diffusion. *arXiv preprint arXiv:2506.17298*, 1, 2025.

Leviathan, Y., Kalman, M., and Matias, Y. Fast inference from transformers via speculative decoding. In *International Conference on Machine Learning*, pp. 19274–19286. PMLR, 2023.

Li, J.-N., Guan, J., Wu, W., and Li, C. Refusion: A diffusion large language model with parallel autoregressive decoding. *arXiv preprint arXiv:2512.13586*, 2025a.

Li, X., Thickstun, J., Gulrajani, I., Liang, P. S., and Hashimoto, T. B. Diffusion-lm improves controllable text generation. *Advances in neural information processing systems*, 35:4328–4343, 2022.

Li, Y., Dong, Z., Sun, Y., Wang, W., Xiong, S., Luo, Y., Liu, J., Lu, H., Wang, J., Su, W., et al. Attention illuminates llm reasoning: The preplan-and-anchor rhythm enables fine-grained policy optimization. *arXiv preprint arXiv:2510.13554*, 2025b.

Lou, A., Meng, C., and Ermon, S. Discrete diffusion language modeling by estimating the ratios of the data distribution. 2023.

Lou, A., Meng, C., and Ermon, S. Discrete diffusion modeling by estimating the ratios of the data distribution. In *Proceedings of the 41st International Conference on Machine Learning*, pp. 32819–32848, 2024.

Men, T., Cao, P., Jin, Z., Chen, Y., Liu, K., and Zhao, J. Unlocking the future: Exploring look-ahead planning mechanistic interpretability in large language models. *arXiv preprint arXiv:2406.16033*, 2024.

Nie, S., Zhu, F., You, Z., Zhang, X., Ou, J., Hu, J., Zhou, J., Lin, Y., Wen, J.-R., and Li, C. Large language diffusion models. *arXiv preprint arXiv:2502.09992*, 2025.

Ou, J., Nie, S., Xue, K., Zhu, F., Sun, J., Li, Z., and Li, C. Your absorbing discrete diffusion secretly models the conditional distributions of clean data. *arXiv preprint arXiv:2406.03736*, 2024.

Prabhudesai, M., Wu, M., Zadeh, A., Fragkiadaki, K., and Pathak, D. Diffusion beats autoregressive in data-constrained settings. *arXiv preprint arXiv:2507.15857*, 2025.

Sahoo, S., Arriola, M., Schiff, Y., Gokaslan, A., Marroquin, E., Chiu, J., Rush, A., and Kuleshov, V. Simple and effective masked diffusion language models. *Advances in Neural Information Processing Systems*, 37:130136–130184, 2024.

Sakaguchi, K., Bras, R. L., Bhagavatula, C., and Choi, Y. Winogrande: An adversarial winograd schema challenge at scale. *Communications of the ACM*, 64(9):99–106, 2021.

Shi, J., Han, K., Wang, Z., Doucet, A., and Titsias, M. Simplified and generalized masked diffusion for discrete data. *Advances in neural information processing systems*, 37:103131–103167, 2024.

Wang, X., Caccia, L., Ostapenko, O., Yuan, X., Wang, W. Y., and Sordoni, A. Guiding language model reasoning with planning tokens. *arXiv preprint arXiv:2310.05707*, 2023.

Wang, X., Xu, C., Jin, Y., Jin, J., Zhang, H., and Deng, Z. Diffusion llms can do faster-than-ar inference via discrete diffusion forcing. *arXiv preprint arXiv:2508.09192*, 2025.

Wang, Y., Ma, X., Zhang, G., Ni, Y., Chandra, A., Guo, S., Ren, W., Arulraj, A., He, X., Jiang, Z., et al. Mmlu-pro: A more robust and challenging multi-task language understanding benchmark. *arXiv preprint arXiv:2406.01574*, 2024.

Wu, C., Zhang, H., Xue, S., Diao, S., Fu, Y., Liu, Z., Molchanov, P., Luo, P., Han, S., and Xie, E. Fast-dllm v2: Efficient block-diffusion llm. *arXiv preprint arXiv:2509.26328*, 2025a.

Wu, C., Zhang, H., Xue, S., Liu, Z., Diao, S., Zhu, L., Luo, P., Han, S., and Xie, E. Fast-dllm: Training-free acceleration of diffusion lilm by enabling kv cache and parallel decoding. *arXiv preprint arXiv:2505.22618*, 2025b.

Wu, S. and Zhang, J. Free draft-and-verification: Toward lossless parallel decoding for diffusion large language models. *arXiv preprint arXiv:2510.00294*, 2025.

Yang, Y., Wang, C., Wang, S., Wen, Z., Qi, B., Xu, H., and Zhang, L. Diffusion lilm with native variable generation lengths: Let [eos] lead the way. *arXiv preprint arXiv:2510.24605*, 2025.

Ye, J., Xie, Z., Zheng, L., Gao, J., Wu, Z., Jiang, X., Li, Z., and Kong, L. Dream 7b: Diffusion large language models. *arXiv preprint arXiv:2508.15487*, 2025a.

Ye, Z., Zhang, Z., Zhang, Y., Ma, J., Lin, J., and Feng, F. Disentangling reasoning tokens and boilerplate tokens for language model fine-tuning. In *Findings of the Association for Computational Linguistics: ACL 2025*, pp. 20939–20957, 2025b.

Yu, R., Ma, X., and Wang, X. Dimple: Discrete diffusion multimodal large language model with parallel decoding. *arXiv preprint arXiv:2505.16990*, 2025.

Zhang, M., Wang, Z., Yang, Z., Feng, W., and Lan, A. Interpretable math word problem solution generation via step-by-step planning. *arXiv preprint arXiv:2306.00784*, 2023.

Zhou, C., Wang, C., Zhang, D., Tong, S., Wang, Y., Bates, S., and Jaakkola, T. Next semantic scale prediction via hierarchical diffusion language models. *arXiv preprint arXiv:2510.08632*, 2025.

Zhu, F., Wang, R., Nie, S., Zhang, X., Wu, C., Hu, J., Zhou, J., Chen, J., Lin, Y., Wen, J.-R., et al. Llada 1.5: Variance-reduced preference optimization for large language diffusion models. *arXiv preprint arXiv:2505.19223*, 2025.

## A. Appendix

### A.1. Planning Tokens

This section delineates the methodology for constructing the set of planning tokens  $\mathcal{P}$ —a vocabulary of high-frequency syntactic and semantic anchors that govern the structural trajectory of the generated sequence. To ensure both coverage and precision, our construction methodology employs a hybrid strategy that integrates *static structural distillation* with the *deterministic discourse anchoring* described subsequently.

**Static List Acquisition via Structural Distillation** Manually curating a comprehensive planning vocabulary is intractable given the diversity of generation contexts. To address this, we utilize a modern Large Language Model (e.g., Gemini 3 Pro) as a *structural distillation engine* to extract a compact, domain-invariant set of tokens. We enforce strict constraints to ensure the generated tokens are content-neutral and syntax-safe, explicitly excluding invisible control characters and variable-specific identifiers. The prompt template used to generate this list is shown below, followed by the static token list returned by Gemini 3 Pro. Notably, the generated static list also includes common reasoning and mathematical operator anchors (e.g.,  $+$ ,  $-$ ), consistent with prior work that studies such markers as planning signals for improved reasoning behavior (Zhang et al., 2023).

Prompt: Generating Planning Tokens

I need a “Planning Token” list for a parallel decoding algorithm of diffusion language models. These tokens act as the structural skeleton of valid code/text. **The Rules (Strict Adherence Required):**

- Content Neutrality:** The list must **ONLY** contain language primitives (keywords, operators, built-ins, standard delimiters). Do **NOT** include variable names (e.g., `i`, `x`, `data`), common string literals, or domain-specific business logic words.
- Syntax Safety:** **EXCLUDE** all invisible formatting or whitespace tokens. Specifically, **NO** newlines (`\n`), tabs (`\t`), carriage returns (`\r`), or solitary whitespace tokens. Every token must be a visible, functional anchor.
- High Frequency:** These must be the most ubiquitous tokens in the language, required for almost any valid file.

**Anchoring Logical Pivots via Sentence-Initial Tokens** In multi-step reasoning domains, specific discourse markers—such as *Therefore*, *Thus*, *However*, or *Step 1*—serve as high-leverage **logical pivots**. These tokens explicitly delimit the structural boundary between a preceding premise and a new deduction. To comprehensively capture these influential anchors without relying on an exhaustive manual list, we implement a deterministic syntactic prior that targets the superset of these markers: all *capitalized initial tokens*. Since capitalization predominantly signals the **sentence-initial position**, this criterion robustly identifies the structural onsets of new reasoning blocks. By treating these sentence starters as planning tokens, our method enforces a **structural lock**, ensuring the model commits to the causal trajectory of the next logical step before generating the dependent semantic content.

**Anchoring the Termination Boundary** Complementing the initiation anchors, we explicitly designate the End-of-Sequence (EOS) token as the definitive **terminal anchor**. In the context of diffusion decoding, the EOS token functions not merely as a cessation signal, but as a critical structural scaffold that delimits the finite boundary of the generation trajectory (Yang et al., 2025). By treating termination as a high-priority planning event, our algorithm acts to **preemptively truncate** the decoding process the instant the logical conclusion is realized. This ensures that the generation trajectory is rigorously bounded, preventing computational expenditure on post-conclusion noise and enforcing a precise structural endpoint to the chain of thought.

## Planning Token Reference List

**1. Control Flow & Structure (The Skeleton)**

```
def, class, return, import, from, as, if, elif, else, for, while, break, continue, pass, try, except, raise, finally, with, assert, lambda, yield, global, nonlocal, del
```

**2. Logical & Comparison Operators (The Decision Makers)**

```
and, or, not, is, in, ==, !=, >=, <=, >, <
```

**3. Critical Punctuation (The Syntax Glue)**

```
:, (, ), [ , ], {, }, , , ->, @
```

**4. Built-in Functions (Action Anchors)**

```
len, range, enumerate, zip, sorted, reversed, int, float, str, list, dict, set, tuple, bool, sum, max, min, abs, round, pow, divmod, print, input, open, map, filter, all, any, isinstance, issubclass, type
```

**5. Common Methods (Data Structure Anchors)**

```
append, extend, insert, remove, pop, clear, index, count, sort, reverse, get, keys, values, items, update, add, union, intersection, difference, split, join, strip, replace, format, startswith, endswith, lower, upper
```

**6. Reasoning, Math, & Comment Anchors**

```
#, =, +, -, *, /, //, %, **, +=, -=, *=, /=
```

**7. Dynamic & Special Anchors (Context-Aware)**

- **End of Text Token (EOS):** (`<|endoftext|>`)
- **Capitalized Initial Words:** Any token starting with a capital letter (e.g., `Therefore`, `If`, `Let`).

## A.2. Additional Details of Ablation Studies

**Ablation setting (Section 3).** We evaluate two exploration variants—*Random* and *Planning*—under the same Semi-Autoregressive Blockwise Decoding framework introduced in Section 2. At each decoding iteration, we proceed as follows.

1. **High-confidence commits.** We first commit all masked positions that satisfy the static Fast-dLLM unmasking rule (Wu et al., 2025b) with threshold  $\tau_{\text{high}} = 0.9$ .
2. **Low-confidence exploration within a confidence bin.** Let  $[\tau^l, \tau^u]$  denote the active confidence range (bin). Among the remaining masked positions in the current active block whose top-1 posterior confidence lies in  $[\tau^l, \tau^u]$ , we commit exactly one additional token using one of the following strategies:
  - (a) **Random.** Uniformly sample one eligible masked position (within the block) and commit its top-1 token.
  - (b) **Planning.** We form the subset of eligible masked positions whose top-1 token is in  $\mathcal{P}$  and whose confidence lies in  $[\tau^l, \tau^u]$ . If this subset is non-empty, we uniformly sample one element from it and commit its top-1 token. If it is empty, we fall back to the same Random rule above (sampling from all eligible positions in  $[\tau^l, \tau^u]$ ).

The fallback in the Planning variant is important for a fair comparison: since  $\mathcal{P}$  is deliberately small, the planning-eligible subset is sometimes empty (see Figure 8). Without a fallback, the Planning variant would make fewer low-confidence commits, confounding accuracy and runtime with a different number of exploration steps. By enforcing a matched exploration rate via fallback, improvements can be attributed to *which* low-confidence tokens are committed (semantic/structural anchors) rather than *how many* are committed.

Additionally, Table A.2 reports the average confidence of the extra lower-confidence tokens committed under both the **Random** and **Planning** strategies. Across all datasets, the average values differ by at most 0.01, indicating that the gains in efficiency and accuracy are driven by prioritizing commits to planning tokens, rather than due to a statistical bias whereby planning tokens exhibit systematically higher posterior confidence within the same confidence band.

**Speedup metric.** We quantify decoding speed by the number of function evaluations (NFE), i.e., the total number of forward passes. For each setting, we report speedup as

$$\text{Speedup} = \frac{\text{NFE}_{\text{Fast-dLLM}}}{\text{NFE}_{(\text{Random/Planning})}},$$

so that larger values indicate fewer forward passes and faster decoding.

Table 2. Comparison of Planning versus Random token strategies in low-confidence regimes. The average confidence (*Avg Token Conf*) of the selected tokens is maintained at comparable levels to ensure a controlled comparison.

Dataset	$\tau^l$	$\tau^u$	Method	Acc.	NFE	Avg. Token Conf.
GSM8K	0.10	0.60	Planning	0.73	50.67	0.38
			Random	0.70	53.97	0.38
	0.15	0.60	Planning	0.74	49.63	0.40
			Random	0.71	51.97	0.39
	0.20	0.60	Planning	0.75	49.78	0.42
			Random	0.72	52.04	0.41
	0.25	0.60	Planning	0.76	50.55	0.43
			Random	0.74	51.89	0.44
HumanEval	0.10	0.60	Planning	0.24	66.38	0.37
			Random	0.18	78.57	0.36
	0.15	0.60	Planning	0.31	67.54	0.39
			Random	0.24	68.74	0.38
	0.20	0.60	Planning	0.30	66.99	0.41
			Random	0.24	70.87	0.40
	0.25	0.60	Planning	0.30	68.90	0.43
			Random	0.26	70.39	0.43

### A.3. Additional Experiments

#### A.3.1. SENSITIVITY ANALYSIS: GENERATION LENGTH AND BLOCK SIZE

To evaluate the robustness of our approach, we benchmark PVF against the Fast-dLLM baseline across varying maximum generation lengths ( $L \in \{256, 512\}$ ) and block sizes ( $k \in \{16, 32, 64\}$ ) on the GSM8K dataset. As shown in Table 3, PVF consistently demonstrates a substantial improvement in algorithmic efficiency, achieving significantly lower NFE than Fast-dLLM across all configurations while maintaining near-identical accuracy. Furthermore, we observe a positive correlation between block size and efficiency gains: as the block size increases, the reduction in NFE becomes more pronounced. This trend validates the efficacy of our planning mechanism, which leverages larger blocks to secure longer verified decoding trajectories, thereby minimizing the number of required forward passes more effectively.

Table 3. Comparison of PVF and Fast-dLLM performance across different Generation Lengths and Block Sizes on GSM8K for LLaDA-8B-Instruct.

Gen Length	Block Size	PVF		Fast-dLLM	
		Accuracy	NFE	Accuracy	NFE
256	16	76.46	37.76	76.30	77.73
	32	75.92	26.75	75.76	71.23
	64	75.84	24.52	75.69	67.85
512	16	79.53	58.34	80.07	110.32
	32	79.92	41.55	79.69	96.86
	64	79.62	31.34	79.62	89.77

#### A.3.2. SENSITIVITY ANALYSIS: PLANNING TOKEN THRESHOLDS $\tau_{\text{PLAN}}^l, \tau_{\text{PLAN}}^u$

We further investigate the sensitivity of PVF to the planning-token thresholds, specifically the lower bound  $\tau_{\text{plan}}^l$  and upper bound  $\tau_{\text{plan}}^u$ . Across the range of values we test, accuracy remains largely stable, indicating that the planning-token procedure

is reasonably reliable. We nonetheless observe a mild trade-off between algorithmic efficiency and generation quality: lowering both threshold bounds consistently reduces NFE (improving efficiency) but leads to a corresponding minor decline in accuracy. This behavior occurs because lowering the thresholds effectively forces the model to commit to planning tokens with lower confidence. While this aggressive commitment typically provides a stronger contextual signal that boosts the confidence of subsequent tokens, which accelerates the decoding process, it simultaneously increases the chance of making mistakes.

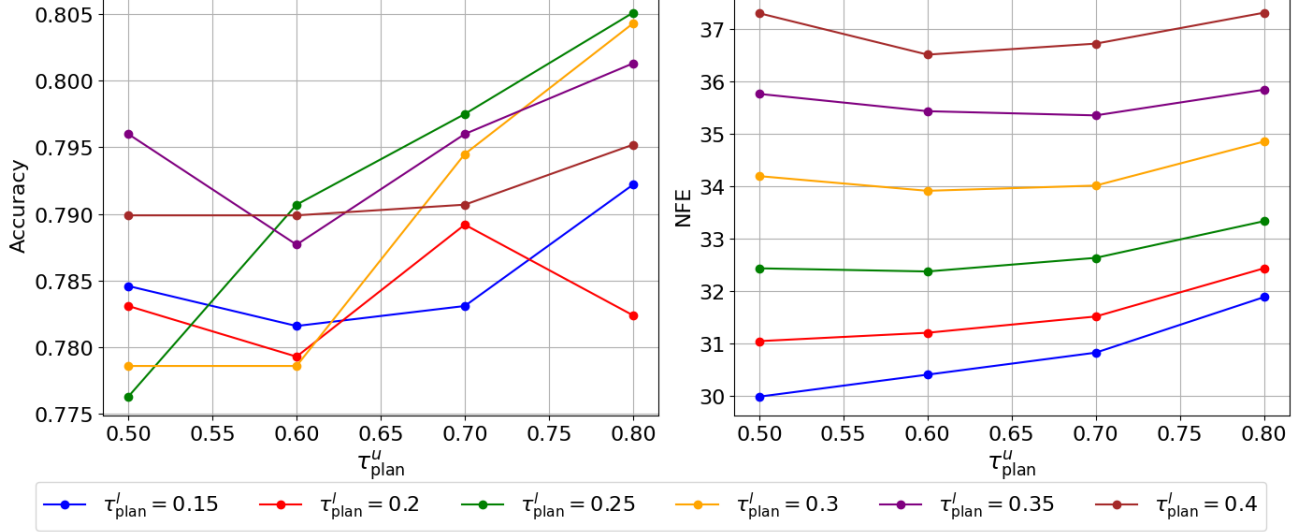


Figure 7. Sensitivity analysis of the planning token threshold. Each line corresponds to a fixed lower bound  $\tau_{\text{plan}}^l$ , plotting accuracy and NFE as a function of the upper bound  $\tau_{\text{plan}}^u$ .

We further examine the percentage of planning tokens relative to the total token count (defined as the sum of planning and AR fallback tokens) under varying lower bound thresholds  $\tau_{\text{plan}}^l$ , while fixing the upper bound at  $\tau_{\text{plan}}^u = 0.9$ . Figure 8 illustrates this relationship, showing that a lower threshold results in a higher proportion of selected planning tokens, which in turn typically leads to better algorithmic efficiency.

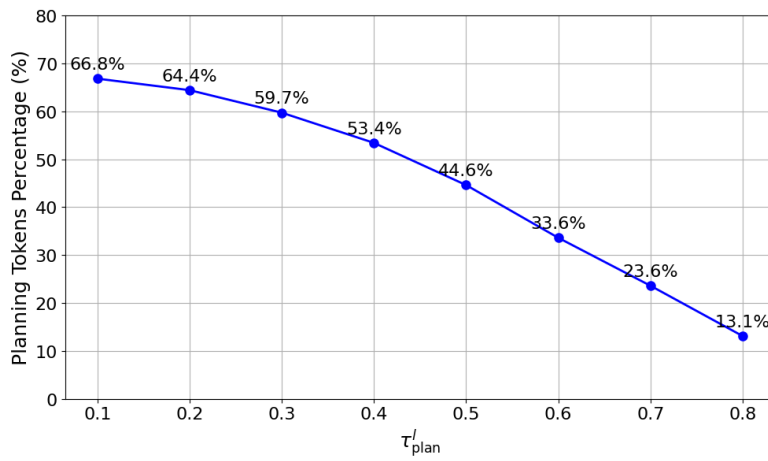


Figure 8. Impact of the planning token threshold lower bound ( $\tau_{\text{plan}}^l$ ) on the percentage of selected planning tokens.

#### A.4. Algorithm Details

---

**Algorithm 1** Plan-Verify-Fill (PVF) Decoding

---

```

1: Input: Model  $P_\theta$ , Sequence Length  $L$ , Thresholds  $\tau_{\text{high}}, \tau_{\text{plan}}$ 
2: Initialize:  $\mathbf{y}_0 \leftarrow [\text{MASK}]^L, t \leftarrow 0$ 
3: while  $\mathbf{y}_t$  contains  $[\text{MASK}]$  do
4:   Construct base state  $\mathbf{z}_t^{\text{base}}$  from  $S_t^{\text{base}}$  as defined in (3)–(4) and identify impact set  $\mathcal{S}_{\text{impact}}(\mathbf{z}_t^{\text{base}}, S_{\text{high conf}})$ .
5:   Route Selection:
6:     Identify planning candidates  $\mathcal{P}_t^{\text{plan}}$  (tokens with sufficient confidence)
7:     if  $\mathcal{P}_t^{\text{plan}} \neq \emptyset$  and PAUSE_FLAG is False then
8:       Choose the Planning Route
9:     else
10:      Choose the AR Fallback Route
11:    end if
12:    Planning Route:
13:      Construct up to 3 candidate trajectories  $\mathbf{z}_t^{\text{plan } 1}, \mathbf{z}_t^{\text{plan } 2}, \mathbf{z}_t^{\text{plan } 3}$ , according to (7). Run parallel forward pass:
14:       $P_\theta \left( \{\mathbf{z}_t^{\text{base}}, \mathbf{z}_t^{\text{plan } 1}, \mathbf{z}_t^{\text{plan } 2}, \mathbf{z}_t^{\text{plan } 3}\} \mid \mathbf{y}_{t-1} \right)$ 
15:      Filter 1: Identify planning trajectories that are consistent with Base on  $\mathcal{S}_{\text{impact}}$  by (8).
16:      if there does not exist a non-contradictory planning trajectory,
17:        Commit  $\mathbf{y}_t = \{\mathbf{z}_t^{\text{base}}\}$ , and set the
18:        PAUSE_FLAG is True, and skip Filter 2.
19:      else
20:        Proceed to Filter 2 below.
21:      end if
22:      Filter 2: Select  $j^*$  among the consistent trajectories that maximizes  $\mathcal{C}_{\text{total}}$ , defined in (9). Commit
23:       $\mathbf{y}_t = \mathbf{z}_t^{\text{plan } j^*}$ .
24:       $t \leftarrow t + 1$ .
25:    Continue
26:    AR Fallback Route:
27:      Construct AR fallback trajectories  $\mathbf{z}_t^{\text{AR } 1}, \mathbf{z}_t^{\text{AR } 2}, \mathbf{z}_t^{\text{AR } 3}$  as defined in (10).
28:      Check consistency with base trajectory  $\mathbf{z}_t^{\text{base}}$  as described in (11).
29:      if there does not exist a non-contradictory planning trajectory,
30:        Commit  $\mathbf{y}_t \leftarrow \mathbf{z}_t^{\text{base}}$ .
31:      else
32:        Select largest  $k$  that  $\mathbf{z}_t^{\text{AR } k}$  is consistent with  $\mathbf{z}_t^{\text{base}}$ , and denote it as  $\mathbf{z}_t^{\text{AR } k^*}$ . Then commit  $\mathbf{y}_t \leftarrow \mathbf{z}_t^{\text{AR } k^*}$ .
33:      end if
34:       $t \leftarrow t + 1$ , set PAUSE_FLAG to False
35:    end while
36:    Return  $\mathbf{y}$ 

```

---

### A.5. Case study

In this section, we present two example generations from LLaDA-8B-Instruct using Fast-dLLM and our PVF strategy. For PVF, we highlight tokens committed via the planning route in yellow and tokens committed via the AR fallback route in pink.

#### LLaDA Prediction of Fast-dLLM (89 steps)

To determine the total number of hours Meredith spent writing articles over the three days, we need to follow these steps:

1. Calculate the number of articles she wrote on Tuesday.
2. Calculate the number of articles she wrote on Wednesday.
3. Find the total number of articles she wrote over the three days.
4. Calculate the total number of hours she spent writing the articles.

\*\*Step 1: Calculate the number of articles she wrote on Tuesday.\*\*

Meredith wrote 5 articles on Monday. On Tuesday, she wrote  $\frac{2}{5}$  times more articles than on Monday. Therefore, the number of articles she wrote on Tuesday is:

$$[ 5 + \frac{2}{5} \times 5 = 5 + 2 = 7 ]$$

\*\*Step 2: Calculate the number of articles she wrote on Wednesday.\*\*

On Wednesday, she wrote twice the number of articles she wrote on Tuesday. Therefore, the number of articles she wrote on Wednesday is:

$$[ 2 \times 7 = 14 ]$$

\*\*Step 3: Find the total number of articles she wrote over the three days.\*\*

The total number of articles she wrote over the three days is the sum of the articles she wrote on Monday, Tuesday, and Wednesday:

$$[ 5 + 7 + 14 = 26 ]$$

\*\*Step 4: Calculate the total number of hours she spent writing the articles.\*\*

Each article takes an average of 4 hours to research and write. Therefore, the total number of hours she spent writing the articles is:

$$[ 26 \times 4 = 104 ]$$

Thus, the total number of hours she spent writing articles in the three days is  $\boxed{104}$ .

LLaDA Prediction with PVF (36 steps)

To determine the total number of hours Meredith spent writing articles over the three days, we need to follow these steps:

1. Calculate the number of articles she wrote on Tuesday.
2. Calculate the number of articles she wrote on Wednesday.
3. Find the total number of articles written each day.
4. Calculate the total number of hours spent writing over the three days.

\*\*Step 1: Calculate the number of articles written on Tuesday.\*\*

Meredith wrote 5 articles on Monday. On Tuesday, she wrote  $\frac{2}{5}$  times more articles than on Monday. Therefore, the number of articles written on Tuesday is:

$$\begin{bmatrix} 5 + \frac{2}{5} \times 5 = 5 + 2 = 7 \end{bmatrix}$$

\*\*Step 2: Calculate the number of articles written on Wednesday.\*\*

On Wednesday, she wrote twice the number of articles she wrote on Tuesday. Therefore, the number of articles written on Wednesday is:

$$\begin{bmatrix} 2 \times 7 = 14 \end{bmatrix}$$

\*\*Step 3: Find the total number of articles written each day.\*\*

- On Monday, she wrote 5 articles.
- On Tuesday, she wrote 7 articles.
- On Wednesday, she wrote 14 articles.

\*\*Step 4: Calculate the total number of hours spent writing over the three days.\*\*

Each article takes an average of 4 hours to research and write. Therefore, the total number of hours spent writing each day is:

- On Monday:  $(5 \text{ articles}) \times 4 \text{ hours/article} = 20 \text{ hours}$
- On Tuesday:  $(7 \text{ articles}) \times 4 \text{ hours/article} = 28 \text{ hours}$
- On Wednesday:  $(14 \text{ articles}) \times 4 \text{ hours/article} = 56 \text{ hours}$

The total number of hours spent writing over the three days is:

$$\begin{bmatrix} 20 \text{ hours} + 28 \text{ hours} + 56 \text{ hours} = 104 \text{ hours} \end{bmatrix}$$

Thus, the total number of hours spent writing articles in the three days is  $(\boxed{104})$ .